arXiv:1605.04771v1 [cond-mat.quant-gas] 9 May 2016

Drag force in bimodal cubic-quintic non-linear Schrödinger equation

David Feijoo, Ismael Ordóñez, Angel Paredes, Humberto Michinel
Área de Óptica, Departamento de Física Aplicada,
Universidade de Vigo, As Lagoas s/n, Ourense, ES-32004 Spain;

We consider a system of two cubic-quintic non-linear Schrödinger equations in two dimensions, coupled by repulsive cubic terms. We analyse situations in which a probe lump of one of the modes is surrounded by a fluid of the other one and analyse their interaction. We find a realization of D'Alembert's paradox for small velocities and non-trivial drag forces for larger ones. We present numerical analysis including the search of static and traveling form-preserving solutions along with simulations of the dynamical evolution in some representative examples.

PACS numbers: 02.30.Jr, 42.65.Tg, 03.75Kk, 42.65.Sf

I. INTRODUCTION

The nonlinear Schrödinger equation (NLSE) is a widely used model in the study of quasi-monochromatic, nonlinear dispersive waves. Among other applications, it describes the dynamics of Bose-Einstein condensates (BECs) in the mean field approximation [1] or the propagation of laser beams in optical fibers [2], for which different expressions have been used for the nonlinearity of the refractive index [3]. The cubic-quintic NLSE [4] is arguably the simplest model for competing nonlinearities [5] and has been used in many different contexts, see *e.g.* [6–9] and references therein. In two transverse dimensions, which is a relevant case for non-linear optics, the cubic (focusing)-quintic (defocusing) model (CQNLSE) presents remarkable features. There are families of stable solitary waves (solitons and vortices) which become flattop when the power of the beam is large: the propagation constant never exceeds a critical value β_{cr} and, for growing power $\beta \to {\beta_{cr}}^-$, there is a growing region where the amplitude also tends to a critical value $\psi \approx e^{i\beta_{cr} z}\psi_{cr}$, as was established by different numerical and analytical methods in [10] and later rigorously proved in [8]. This behaviour endows the flattop solutions of the CQNLSE with the properties of a liquid [11]. The $|\psi| \approx \psi_{cr}$ is a region of constant pressure and the rapid decay from $|\psi| \approx \psi_{cr}$ to $|\psi| \approx 0$ can be identified with a liquid-vapour interface characterized by a surface tension, leading to effects analogous to capillarity and dripping in regular liquids [12]. Remarkably, the first neat experimental realization of this liquid of light has been reported recently [13], following the proposal of [14] of engineering the desired optical properties in a coherent medium.

A natural question is whether there are other hydrodynamical properties that can be defined for this kind of solutions of the CQNLSE. In this paper we analyse the drag, namely the force which opposes to the motion of an object within a surrounding fluid. An "object" inside the fluid described by a NLSE can be modelled by implementing appropriate boundary conditions at the edge of the moving body, as was done in the framework of superfluidity in [7, 15], where similar questions to those addressed here were studied. We will consider a different approach which might be suitable for nonlinear optics or BECs: the probe object is also described by a CQNLSE, leading to a bimodal system of coupled equations for two wave-functions ψ_1, ψ_2. In non-linear optics [16], the ψ_i typically correspond to different polarizations or different carrier wavelengths while in BECs they represent different atomic species in the condensate [17] or different internal states of the same isotope [18], see *e.g.* [19] and references therein.

The system of equations we will study is the following:

$$\begin{aligned} -i\partial_z\psi_1 &= \nabla^2\psi_1 + (|\psi_1|^2 - |\psi_1|^4 - \gamma\,|\psi_2|^2)\psi_1 \\ -i\partial_z\psi_2 &= \nabla^2\psi_2 + (|\psi_2|^2 - |\psi_2|^4 - \gamma\,|\psi_1|^2)\psi_2 \end{aligned} \qquad (1)$$

where for simplicity we have fixed to unity several coefficients. The laplacian is taken over two transverse dimensions $\nabla^2 = \partial_x^2 + \partial_y^2$. For the crossed interaction, we only introduce cubic terms weighed by a constant γ. We will restrict ourselves to analysing $\gamma > 0$, namely inter-modal repulsion resulting in a fluid with inmiscible phases, which is the most suitable situation to formulate thought experiments regarding drag forces.

A bimodal cubic-quintic model similar to (1) was first introduced in [20] to discuss the interaction between solitons of both species. Variations of this model were later used for the study of vector solitons [21], their dynamics [22] and modulational instability [23, 24]. It is worth pointing out that these works mostly deal with inter-modal attraction $\gamma < 0$. An exception is [24], which deals with BECs where interspecies forces can be tuned using Feshbach resonances and can be either attractive or repulsive.

In Eqs. (1), the norm $\int |\psi_i|^2 dxdy$ for each species is conserved separately upon evolution in z. Moreover, it is straightforward to check that total momentum is preserved:

$$\vec{p} = \frac{1}{2i}\int \sum_{i=1,2} \left(\psi_i^*\vec{\nabla}\psi_i - \psi_i\vec{\nabla}\psi_i^*\right) dx\,dy \qquad (2)$$

but the $\vec{p}_i$ associated to each species are not separately conserved, *i.e.*, momentum can be transferred between

species, leading to inter-modal macroscopic forces. In the following, we will consider the dynamics of a droplet of ψ_1 surrounded by a large background of ψ_2, with $\int |\psi_2|^2 dS \gg \int |\psi_1|^2 dS$. We thus study the effects of the drag force exerted by the ψ_2-fluid on an ψ_1-probe "object".

In section II, we discuss the static solutions. In section III, we find form-preserving traveling solutions which can be interpreted as dragless motion of an object within an inviscid fluid and are therefore related to D'Alembert's paradox. These configurations exist below some limiting velocity. We also discuss how this kind of solutions can be approached in processes with dynamical evolution. In section IV, we devise a kind of thought falling ball viscometer experiment and introduce an approximate analogy between this intricate nonlinear setup and a simple mechanical system. In section V, we consider a case in which both species are initially separated and show the similarity of simulated processes with the entrance of a rigid object in a liquid. Finally, we present our conclusions in section VI.

II. STATIC SOLUTIONS

We start by looking for radially symmetric, stationary solutions with a circle of ψ_1 surrounded by an infinite critical background of ψ_2, with $\int |\psi_2|^2 dS = \infty$. Namely:

$$\psi_1 = e^{i\,\beta_1\,z} f_1(r)\,, \qquad \psi_2 = e^{i\,\beta_{cr}\,z} f_2(r) \tag{3}$$

where $f_1(r)$, $f_2(r)$ are real functions and $\beta_{cr} = \frac{3}{16}$ [8]. The system (1) is reduced to:

$$\begin{aligned} \partial_r^2 f_1 + r^{-1}\partial_r f_1 &= \beta_1 f_1 - (f_1^2 - f_1^4 - \gamma f_2^2) f_1\ , \\ \partial_r^2 f_2 + r^{-1}\partial_r f_2 &= \beta_{cr} f_2 - (f_2^2 - f_2^4 - \gamma f_1^2) f_2\ . \end{aligned} \tag{4}$$

Boundary conditions at infinity are:

$$\lim_{r\to\infty} f_1(r) = 0\,, \qquad \lim_{r\to\infty} f_2(r) = \psi_{cr} = \sqrt{3}/2 \tag{5}$$

The profile of the functions at $r \to \infty$ consistent with (5) can be found by computing the leading terms in (4). We find that $f_1(r) \sim r^{-1/2}\exp(-\sqrt{\beta_1 + 3\gamma/4}\,r)$. Therefore, solutions can only exist for $-\frac{3}{4}\gamma < \beta_1$. The function f_2 behaves as $\sqrt{3}/2 - f_2(r) \sim r^{-1/2}\exp(-\sqrt{3}r/2)$ if $\beta_1 > \frac{3}{16}(1-4\gamma)$ and as $\sqrt{3}/2 - f_2(r) \sim \exp(-2\sqrt{\beta_1 + 3\gamma/4}\,r)$ for $\beta_1 \le \frac{3}{16}(1-4\gamma)$.

At $r = 0$, solutions must be regular $f_1'(0) = f_2'(0) = 0$. By performing a Taylor expansion, we find that near the origin the functions can be written in terms of two constants:

$$\begin{aligned} f_1(r) &= a_0 + \frac{a_0}{4}(\beta_1 - a_0^2 + a_0^4 + \gamma\, b_0^2) r^2 + \mathcal{O}(r^4) \\ f_2(r) &= b_0 + \frac{b_0}{4}(\frac{3}{16} - b_0^2 + b_0^4 + \gamma\, a_0^2) r^2 + \mathcal{O}(r^4) \end{aligned}$$

For a given γ, numerical solutions of (4), (5) can be found by rewriting the equations in a finite differences scheme and solving the resulting non-linear algebraic system by standard methods. There is a one-parameter family of nodeless monotonic solutions ($f_1'(r) < 0$ and $f_2'(r) > 0\ \forall r > 0$) with $-\frac{3}{4}\gamma < \beta_1 < \frac{3}{16}$. In the limit $\beta_1 \to \frac{3}{16}$, the norm of ψ_1 diverges and one has a kink-antikink solution with two separate "liquids". Naming r_* the radius of the region where $f_1(r)$ dominates, we have $r_* \to \infty$ as $\beta_1 \to \frac{3}{16}$, $f_1(r) \approx \psi_{cr}$ for $r \ll r_*$ and $f_1(r) \approx 0$ for $r \gg r_*$ and viceversa for $f_2(r)$.

Figure 1 shows three examples of $f_1(r)$, $f_2(r)$ pairs computed numerically. In Fig. 2, we depict the values $f_1(0) = a_0$, $f_2(0) = b_0$ for the families of solutions with $\gamma = 1$ and $\gamma = 2$.

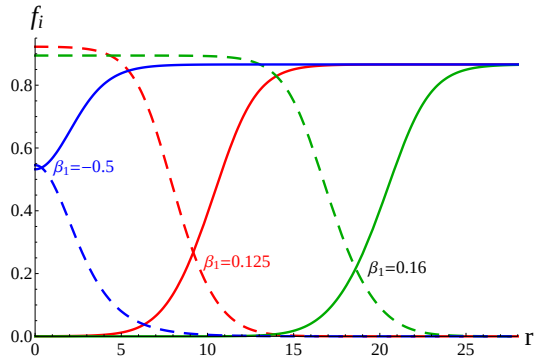

FIG. 1: Solutions of (4), (5) with $\gamma = 1$ for $\beta_1 = -0.5$, $\beta_1 = 0.125$ and $\beta_1 = 0.16$. For larger β_1, the value r_* at which $f_1(r)$ decays and $f_2(r)$ rises increases and, therefore the normalization $\int |\psi_1|^2 dS$ also grows. Dashed lines correspond to $f_1(r)$ and solid lines to $f_2(r)$.

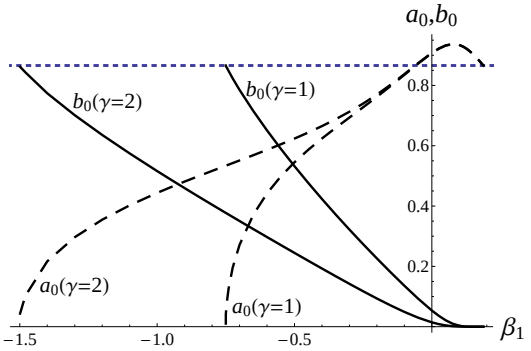

FIG. 2: Values of $f_1(0) = a_0$ (dashed lines) and $f_2(0) = b_0$ (solid lines) computed from the numerical solutions for the families computed taking $\gamma = 1$ and $\gamma = 2$. The horizontal dotted line marks $\psi_{cr} = \sqrt{3}/2$.

In the following sections, we will take $\gamma = 1$. The qualitative results hold for more general values of $\gamma > 0$.

III. D'ALEMBERT'S PARADOX

We now show that there exist solutions in which the lump of the first species moves with constant velocity U within the fluid of the second species, *i.e.* there are situations in which the drag force is exactly zero. They correspond to steady flows in the moving reference frame. A similar behaviour involving a different NLSE model was first found in [15]. Notice that we abuse of language using the word velocity to refer to derivatives with respect to z, which in the nonlinear optics framework correspond to propagation distance rather than time. In that case, the variations in z are a consequence of having non-trivial components of the wave-vector apart from k_z and this velocity is, physically, the propagation angle with respect to the z-axis. We introduce an ansatz of the form:

$$\begin{aligned} \psi_1 &= e^{i\,\beta_U\,z}\phi_1(x, y - U\,z)\,, \\ \psi_2 &= e^{i\,\beta_{cr}\,z}\phi_2(x, y - U\,z)\,, \end{aligned} \tag{6}$$

This system of equations can be treated along the lines of [25]: consider $\eta = y - U\,z$ and write the system as a PDE in x, η. One finds the following:

$$\begin{aligned} iU\partial_\eta\phi_1 &= \nabla^2\phi_1 + \left(|\phi_1|^2 - |\phi_1|^4 - \gamma|\phi_2|^2 - \beta_U\right)\phi_1 \\ iU\partial_\eta\phi_2 &= \nabla^2\phi_2 + \left(|\phi_2|^2 - |\phi_2|^4 - \gamma|\phi_1|^2 - \beta_{cr}\right)\phi_2 \end{aligned} \tag{7}$$

where ∇^2 should now be understood as $\partial_x^2 + \partial_\eta^2$. Boundary conditions at infinity ($x^2 + \eta^2 \to \infty$) are $\phi_1 \to 0$, $\phi_2 \to \sqrt{3}/2$. We split real and imaginary parts as:

$$\phi_1 = \phi_{1R} + i\,\phi_{1I}\,, \qquad \phi_2 = \phi_{2R} + i\,\phi_{2I} \tag{8}$$

The system (7) is invariant under $x \to -x$ and under $\eta \to -\eta$ together with $\phi_{1I} \to -\phi_{1I}$, $\phi_{2I} \to -\phi_{2I}$. Thus, it is enough to compute the functions for $x > 0$, $\eta > 0$ and solutions must be consistent with the following set of Neumann and Dirichlet boundary conditions at $x = 0$ and $\eta = 0$:

$$\begin{aligned} 0 &= \partial_x\phi_{1R}|_{x=0} = \partial_x\phi_{2R}|_{x=0} = \partial_x\phi_{1I}|_{x=0} = \partial_x\phi_{2I}|_{x=0} \\ 0 &= \partial_\eta\phi_{1R}|_{\eta=0} = \partial_\eta\phi_{2R}|_{\eta=0} \\ 0 &= \phi_{1I}|_{\eta=0} = \phi_{2I}|_{\eta=0} \end{aligned} \tag{9}$$

We have found numerical solutions of the problem (7), (9) by using a finite difference method: we discretize the $x-\eta$ plane in a lattice of $N_x \times N_\eta$ points and write down the resulting (approximately) $4N_xN_\eta$ algebraic nonlinear equations for the same number of real variables. Given a judicious initial ansatz, solutions can be found by a standard Newton-Raphson method. For fixed γ, there is a two-parameter family of solutions, depending on U and β_U. Since the solutions with $U = 0$ have been computed in section II, they are a good starting point to search for different solutions of the family. In particular, we are interested in solutions with different U's but constant $\int |\phi_1|^2 dx\, d\eta$. The relation of β_U with the norm is non-trivial, but, for fixed U, we can vary β_U and compute different solutions until we get the one with the desired normalization. For fixed normalization, there is a maximal value of $|U|$ for which the solution exists.

A few examples of numerical approximations — computed in a 120×240 lattice — are depicted in Fig. 3. We depict contour maps of the quantity $|\phi_1|^2 + |\phi_2|^2$. It should be understood that the inner region mostly corresponds to $|\phi_1|^2$ and the outer one to $|\phi_2|^2$. The region where $|\phi_1|^2 + |\phi_2|^2$ drastically descends is the interface. The plots show how the $|\phi_i|^2$-distributions of the traveling solutions get deformed as the velocity is increased.

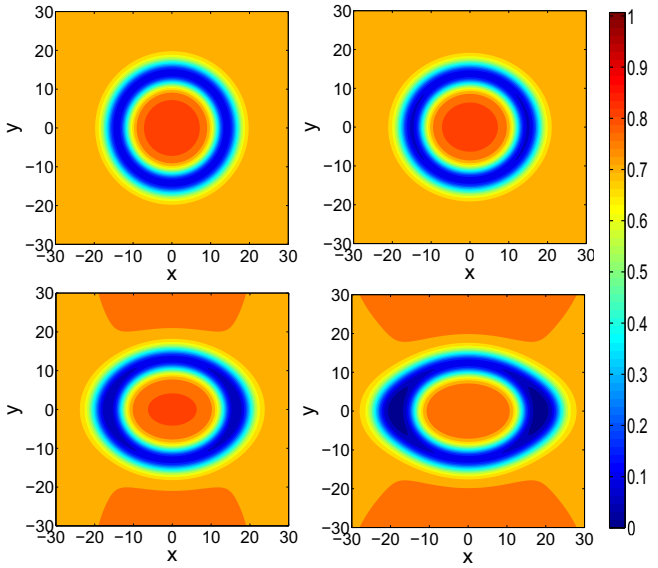

FIG. 3: Contour plots of $|\phi_1|^2+|\phi_2|^2$ for four solutions of Eqs. (7) with $\int |\phi_1|^2 dx\, d\eta \approx 355$. This normalization corresponds to $\beta_1 = 0.15$ in the formalism of section II. The four images correspond to $U = 0$; $U = -0.1$; $U = -0.15$; $U = -0.17$; respectively.

It is also interesting to understand what happens if the initial conditions do not correspond exactly to these stationary solutions. With that aim, we have performed simulations in which the static solutions of section II are given a boost, *i.e.*, ψ_1 is multiplied by $e^{-i\,u_0\,y/2}$ where u_0 is (minus) the initial velocity and then used as initial conditions in (1). The evolution is computed by a standard split-step pseudo-spectral method, the so-called beam propagation method. In order to avoid spurious effects related to boundary conditions, we have taken a finite droplet for the second species. Simulations [27] show that, initially, the boosted soliton loses momentum to the medium but eventually tends to a constant velocity, approaching the above described behaviour related to D'Alembert's paradox.

In order to describe this effect quantitatively, let us

define the central position of the ψ_1 droplet as:

$$\langle y_1\rangle(z) = \frac{\int\int y|\psi_1(z)|^2 dxdy}{\int\int |\psi_1(z)|^2 dxdy} \qquad (10)$$

and its velocity as $u(z) = -\frac{d\langle y_1\rangle(z)}{dz}$. Figure 4 shows how u evolves upon propagation for different examples.

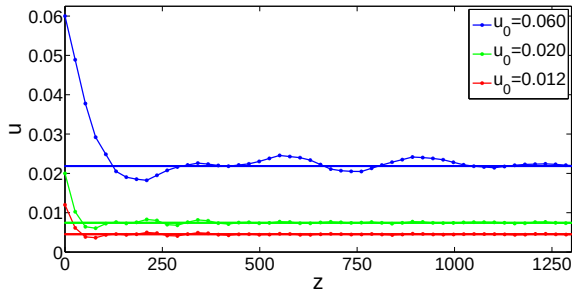

FIG. 4: Examples of the evolution with z of the velocity of the first species lump immersed in the dragging fluid. The horizontal lines mark the asymptotic velocity inferred from the simulations.

IV. TERMINAL VELOCITY AND DRAG FORCE

We now devise a thought experiment which can be considered an NLSE version of the evolution of a body moving within a fluid subject to an external force. Let us modify (1) to include an extra term accounting for a potential acting on ψ_1 along the y-direction — which in the case of optics would correspond to a linear variation of the linear refractive index:

$$\begin{aligned} -i\partial_z\psi_1 &= \nabla^2\psi_1 + (|\psi_1|^2 - |\psi_1|^4 - \gamma\,|\psi_2|^2)\psi_1 - g\,y\,\psi_1 \\ -i\partial_z\psi_2 &= \nabla^2\psi_2 + (|\psi_2|^2 - |\psi_2|^4 - \gamma\,|\psi_1|^2)\psi_2 \end{aligned} \qquad (11)$$

We will consider an initially static solution as discussed in section II, for which g is eventually turned on, namely $g = 0$ for $z < 0$ and is shifted to a constant for $z > 0$. We compute this evolution by numerically integrating (4) by the split-step pseudo-spectral beam propagation method. The ψ_1 distribution starts drifting driven by g but the drag force of the fluid eventually stops the acceleration and the motion tends to a terminal velocity $u_T(g)$.

The qualitative behaviour is different for small and large g. For large g, a void is generated in the wake of the moving object. For smaller g, vortex-antivortex pairs get detached from this void, contributing to the drag force. This behaviour is parallel to the one described in [7] for the case in which a superfluid modelled by a cubic-quintic equation flows past a rigid obstacle. It is worth mentioning that the confluence of the liquid which isolates the vortex and antivortex from the void generated by the moving object qualitatively resembles a splash singularity [26], even if the mathematical details are rather different.

Notice that, as also happened in the set-up of section III, the initially round ψ_1-distribution gets somewhat deformed. As it could be expected, the deformation is greater when larger velocities are reached. Moreover, for large velocities, the surface tension forces of the surrounding liquid fail to rapidly occupy the void left at the object's trail and a bubble is generated. Figures 5 and 6 show representative examples, see also [27].

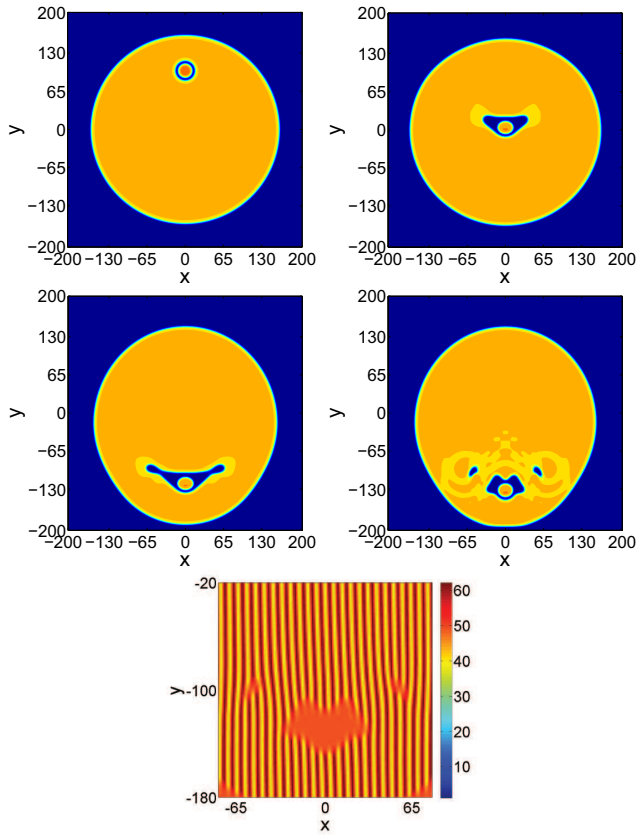

FIG. 5: Evolution with $g = 8\times10^{-4}$. The initial configuration is the static solution with $\beta_1 = 0.15$. The four first images correspond to $z = 0$, 800, 1900 and 2000, respectively, and their color convention is as in Fig. 3. The terminal velocity is moderate and the moving object leaves a trail of vortex-antivortex pairs, whose nucleation and detachment contribute to the drag force. The plot below explicitly shows the phase singularities of the vortex and antivortex, which appear as fork-like structures in the interference pattern of the wave-function with a plane wave. Concretely, the image corresponds to $|\psi_2(z = 2000) + 7\exp(1000\,i\,x)|^2$.

In this set-up, it is possible to compute numerically the terminal velocity for different values of g and different initial functions ψ_1, corresponding to different values of β_1 as defined in section II. We restrict ourselves to values of β_1 not far from β_{cr} in order to have distributions

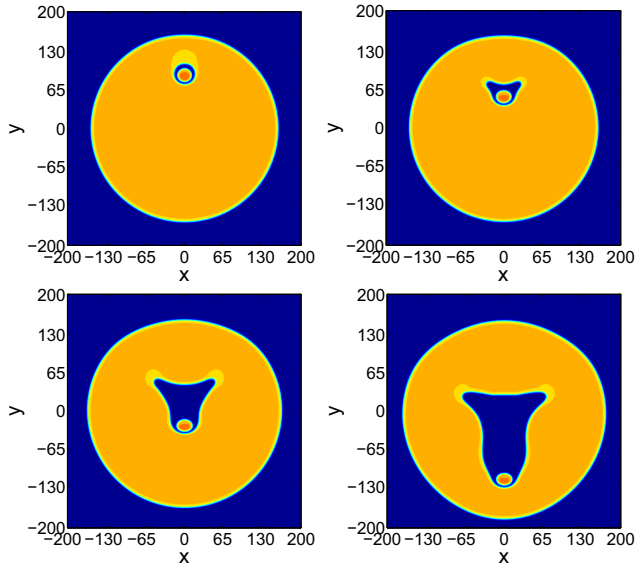

FIG. 6: Evolution with $g = 2 \times 10^{-3}$. The four images correspond to $z = 100$, 300, 600 and 900, respectively. Colors are as in Fig. 3. The terminal velocity is larger than in the previous case and the advance of the lump of the first species leaves a bubble at its wake.

of ψ_1 for which the analogy to a body within a fluid is applicable to some extent. We plot some results in figure 7.

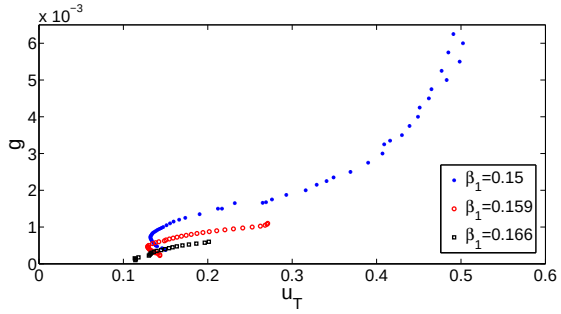

FIG. 7: Some examples of $g(u_T)$.

As $g \to 0$ the value of u_T tends to a positive constant, as it could be expected from the D'Alembert's paradox behaviour. This result is reminiscent of [15], even if the set-up is rather different. For large values of g, the drag becomes quadratic in velocity. When β_1 is very near β_{cr}, the quadratic drag regime already starts at small velocities. Presumably, the reason is that the lump becomes more malleable in this regime yielding a modification of the qualitative behaviour.

For certain ranges of g and different values of β_1, the results can be approximated by straight lines (notice however that for small g, u_T can decrease with increasing g). This linear growth suggests the possibility of considering a simple modelling of the situation in which the drag force is just considered linear in velocity. A body subject to a constant force and a quadratic drag force satisfies $\frac{d\langle y_1\rangle}{dz} = -g + k\,u$, which gives $\langle y_1\rangle = -\frac{g}{k^2}(k\,z + e^{-k\,z} - 1)$. We have compared the numerically computed trajectories $\langle y_1(z)\rangle$ to fits of the form

$$\langle y_1(z)\rangle = -a(b\,z + e^{-b\,z} - 1) \tag{12}$$

where a and b are taken as free parameters. It turns out that the simple mechanical model is rather precise for the setup of the present section in a large range of parameters. This cannot be an exact characterization of the

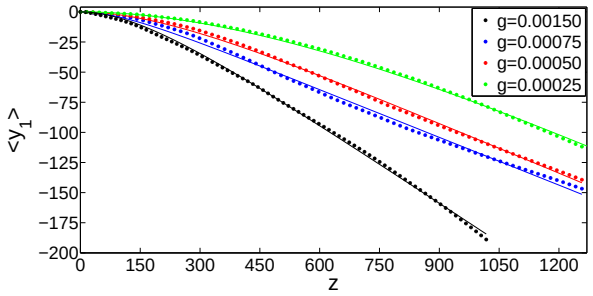

FIG. 8: Examples of comparison of $\langle y_1\rangle(z)$ computed numerically (dots) with fits to the simple model (12) (solid lines). In all cases the initial conditions use the $\beta_1 = 0.15$ solution of section II.

system for several reasons: first of all, we have seen in section III that there are dragless flows and (12) fails to describe them. Indeed, a more complicated dependence of the drag force on u was found in Fig 7, which could be introduced in the mechanical model at the cost of losing simplicity. Moreover, since the "object" itself gets deformed while propagating, its interaction with the environment should depend on its form too. This explains, for instance, the mild oscillations of the simulated motion in Fig. 8 around the solid lines. As the β_1 of the initial distribution deviates away from β_{cr}, the precision of the simple modelling (12) declines.

V. INITIALLY SEPARATED SPECIES

Up to now, we have considered situations in which species 1 is initially within the fluid. In this section, we illustrate the case in which both species are separated at the outset while afterwards, the soliton of species 1 enters the bulk of species 2. Concretely, we consider equation Eqs. (1) with a linear potential term $-g\,y\,\psi_i$ for both species. For species 2, we also include a potential barrier at the bottom. Periodic boundary conditions are considered in the x-direction. The evolution is depicted in Fig. 9, see also [27]. We observe that the collision produces surface and body waves. Due to the analogy to a system

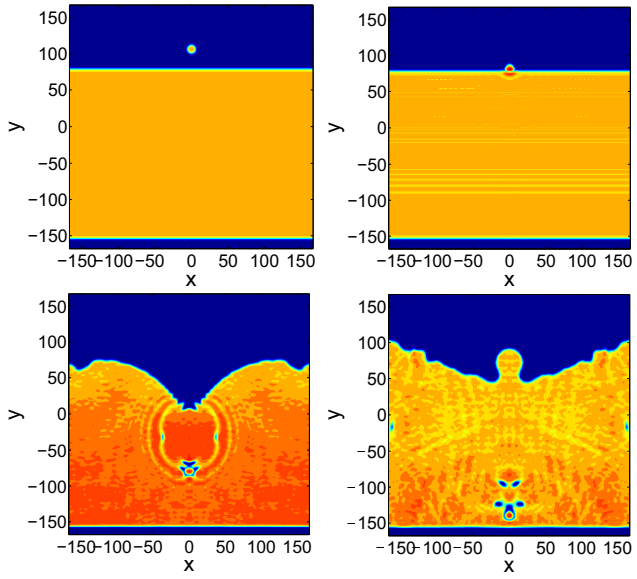

FIG. 9: A soliton entering the bulk of a fluid, as described by a bimodal system of cubic-quintic non-linear Schrödinger equations. The different images correspond to $z = 10, 50, 500, 700$ in the simulation. Colors are as in Fig. 3.

with surface tension of the cubic-quintic equations, the behaviour at the surface resembles that of a liquid hit by an object. Once the soliton enters the liquid, it starts experiencing a drag force as described in the previous sections. The simulation shows the eventual nucleation of vortex-antivortex pairs related to this friction process, see the last image in Fig. 9. Moreover, since the liquid is somewhat stirred, dark solitary traveling waves (namely, rarefaction pulses [9, 25]) can be excited. Two of them moving horizontally in opposite directions can be seen in the plots.

VI. CONCLUSIONS

We have analysed a coupled system of cubic-quintic nonlinear Schrödinger equations in order to understand drag forces in physical systems that can be modelled as fluids within this formalism, such as the so-called liquid light or certain Bose-Einstein condensates. The two equations correspond to having two modes, such as transverse polarizations for light or different atomic species. A lump of one of the species immersed in a larger fluid of the other is subject to macroscopic forces that influence its dynamics. For small velocities, there are situations in which a D'Alembert's paradox situation exists, namely the lump moves preserving its form and velocity. Notice however that it would be wrong to say that it is unaffected by the inviscid fluid, since the energy distribution of the first species does depend on its velocity, as shown in Fig. 3. For larger velocities, the drag forces set in. Roughly, it can be said that they grow linearly with u in a certain region and then grow quadratically for larger u. It is possible to establish an approximate mechanical analogy and consider that the system is just described by a simple equation for a rigid object subject to a force which only depends on velocity. This modelling is accurate to some extent but it is obviously limited since for instance it disregards deformations of both the fluid and the object as described by the CQNLSEs, which also alter the macroscopic dynamics. Overall, these results give further evidence of the qualitative resemblance of physical systems modelled by the CQNLSE to ideal liquids.

Acknowledgements.- We thank D. Nóvoa for discussions and comments on the manuscript. The work of AP is supported by the Ramón y Cajal program. The work of DF is supported by the FPU Ph.D. program. The work of DF, IO and AP is also supported by Xunta de Galicia through grant EM2013/002.

[1] F. Dalfovo, S. Giorgini, L.P. Pitaevskii, and S. Stringari, Rev. Mod. Phys. **71**, 463 (1999).
[2] G.P. Agrawal, *Nonlinear Fiber Optics* 4th Ed., Elsevier/Academic Press, 2006.
[3] Y.S. Kivshar, B. Luther-Davies, Phys. Rep. **298** (1998), 81-197.
[4] J. Herrmann, Opt. Comm. **91** (1992) 337-340. F.G. Bass, V.V. Konotop, and S.A. Puzenko, Phys. Rev. A **46**, 4185 (1992). V. Królikowski, N. Akhmediev and B. Luther-Davies, Phys. Rev. E **48**, 3980 (1993).
[5] A.H. Piekara, J.S. Moore and M. S. Feldt, Phys. Rev. A **9**, 1403 (1974).
[6] I.V. Barashenkov, E.Y. Panova, Physica D **69** (1993) 114-134. C. Josserand and S. Rica, Phys. Rev. Lett. **78**, 1215 (1997). T. A. Davydova, A. I. Yakimenko, and Yu. A. Zaliznyak, Phys. Rev. E **67**, 026402 (2003). B.B. Baizakov, A. Bouketir, A. Messikh, A. Benseghir, B.A. Umarov, Int. Jour. Mod. Phys. B **25**, 2427-2440 (2011). R.M. Caplan, R. Carretero-Gonzalez, R. Kevrekidis, B.A. Malomed, Math. Comp. Simul. **82**, 1150-1171 (2012). C. Trallero-Giner, R. Cipolatti, T.C. H. Liew, Eur. Phys. J. B **67**, 143 (2013).
[7] C. Josserand, Y. Pomeau, S. Rica, Phys. Rev. Lett. **75**, 3150-3154 (1995).
[8] V. Prytula, V. Vekslerchik, and V. M. Pérez-García, Phys. Rev. E **78**, 027601 (2008).
[9] A. Paredes, D. Feijoo, H. Michinel, Phys. Rev. Lett. **112**, 173901 (2014).
[10] K. Dimitrevski *et al.*, Phys. Lett A **248** (1998) 369-376. V.I. Berezhiani, V. Skarka and N. B. Aleksic, Phys. Rev E **64**, 057601 (2001). R.L. Pego and H.A. Warchall, J. Nonlinear Sci. **12**, 347394 (2002). H. Michinel, J.R. Salgueiro, M.J. Paz-Alonso, Phys. Rev. E **70**, 066605 (2004).
[11] D. E. Edmundson and R. H. Enns, Phys. Rev. A **51**, 2491 (1995). M. Quiroga-Teixeiro and H. Michinel, J. Opt. Soc. Am. B **14**, 2004 (1997). D. Mihalache et al., Phys. Rev. Lett. **88**, 073902 (2002). H. Michinel, J. Campo-Táboas, R. García-Fernández, J. R. Salgueiro, and M. L. Quiroga-Teixeiro, Phys. Rev. E **65**, 066604 (2002). M. J. Paz-Alonso, D. Olivieri, H. Michinel, and J. R. Salgueiro,

Phys. Rev. E **69**, 056601 (2004).
[12] D. Novoa, H. Michinel, D. Tommasini, Phys. Rev. Lett. **103**, 023903 (2009).
[13] Z. Wu, Y. Zhang, C. Yuan, F. Wen, H. Zheng, Y. Zhang, M. Xiao, Phys. Rev. A **88**, 063828 (2013).
[14] H. Michinel, M. J. Paz-Alonso, V. M. Pérez-García, Phys. Rev. Lett **96**, 023903 (2006). A. Alexandrescu, H. Michinel, V. M. Pérez-García, Phys. Rev. A **79**, 013833 (2009).
[15] T. Frisch, Y. Pomeau and S. Rica, Phys. Rev. Lett. **69**, 1644 (1992).
[16] S. V. Manakov, Zh. Eksp. Teor. Fiz. **65**, 505 (1973) [Sov. Phys. JETP **38**, 248 (1974)].
[17] G. Modugno, M. Modugno, F. Riboli, G. Roati, and M. Inguscio, Phys. Rev. Lett. **89**, 190404 (2002).
[18] C. J. Myatt, E. A. Burt, R. W. Ghrist, E. A. Cornell, and C. E. Wieman, Phys. Rev. Lett. **78**, 586 (1997).
[19] X. Liu, H. Pu, B. Xiong, W. M. Liu, and J. Gong, Phys. Rev. A **79**, 013423 (2009). G. Csire, D. Schumayer, and B. Apagyi, Phys. Rev. A **82**, 063608 (2010). Z. M. He, D. L. Wang, J. W. Ding, and X. H. Yan, Eur. Phys. J. D **66**, 139 (2012). D. Feijoo, A. Paredes and H. Michinel Phys. Rev. A **87**, 063619 (2013).
[20] A. Maimistov, B. Malomed, A. Desyatnikov, Phys. Lett. A **254** (1999), 179-184.
[21] D. Mihalache, D. Mazilu, I. Towers, B.A. Malomed, F. Lederer, J. Opt. A: Pure Appl. Opt. **4** 615 (2002). D. Mihalache, D. Mazilu, I. Towers, B.A. Malomed, F. Lederer, Phys. Rev. E **67** 056608 (2003). D. Mihalache, D. Mazilu, B.A. Malomed, F. Lederer, J. Opt. B: Quantum Semiclass. Opt. **6** S341 (2004). A. S. Desyatnikov, D. Mihalache, D. Mazilu, B. A. Malomed, C. Denz, and F. Lederer. Phys. Rev. E **71**, 026615 (2005). J. M. Alcaraz-Pelegrina, P. Rodriguez-Garcia, Phys. Lett. A **374**, 1591 (2010). P. Wang, B. Tian, Opt. Comm. **285**, 3567 (2012).
[22] P. Wang, B. Tian, Jour. Mod. Opt. **59**, 1786 (2012).
[23] J. M. Alcaraz-Pelegrina, P. Rodriguez-Garcia, Phys. Lett. A **375**, 2815 (2011).
[24] B. B. Baizakov, A. Bouketir, A. Messikh, B. A. Umarov, Phys. Rev. E **79**, 046605 (2009).
[25] C.A. Jones, P.H. Roberts, J. Phys. A: Math. Gen. **15** (1982), 2599-2619. C.A. Jones, S.J. Putterman, P.H. Roberts, J. Phys. A: Math. Gen. **19** (1986), 2991-3011. D. Chiron, C. Scheid, preprint HAL-Inria Open Archive hal-00873794 (2013) (http://hal.archives-ouvertes.fr/docs/00/87/37/94/PDF/Endim2.pdf
[26] A. Castro, D. Córdoba, C.L. Fefferman, F. Gancedo and J. Gómez-Serrano, PNAS **109**, 733-738 (2012).
[27] See Supplemental Material for animations of several simulations.